Role of Individual Surface Charges of Voltage-Gated K Channels

Fredrik Elinder and Peter Århem
The Nobel Institute for Neurophysiology, Department of Neuroscience, Karolinska Institutet, S-171 77 Stockholm, Sweden

ABSTRACT Fixed charges on the extracellular surface of voltage-gated ion channels influence the gating. In previous studies of cloned voltage-gated K channels, we found evidence that the functional surface charges are located on the peptide loop between the fifth transmembrane segment and the pore region (the S5–P loop). In the present study, we determine the role of individual charges of the S5–P loop by correlating primary structure with experimentally calculated surface potentials of the previously investigated channels. The results suggest that contributions to the surface potential at the voltage sensor of the different residues varies in an oscillating pattern, with the first residue of the N-terminal end of the S5–P loop, an absolutely conserved glutamate, contributing most. An analysis yields estimates of the distance between the residues and the voltage sensor, the first N-terminal residue being located at a distance of 5–6 Å. To explain the results, a structural hypothesis, comprising an α-helical N-terminal end of the S5–P loop, is presented.

INTRODUCTION

Fixed external surface charges of voltage-gated ion channels have been shown to influence gating (Frankenhaeuser and Hodgkin, 1957), conductance (Frankenhaeuser, 1960; Sigworth and Spalding, 1980), and toxin binding (Baker and Rubinson, 1975; MacKinnon and Miller, 1989). The location of the charges affecting conductance and toxin binding has been extensively studied (see Doyle et al., 1998 for a structural model of a K channel), whereas much less is known about charges affecting gating. Because the Debye length under physiological conditions (9 Å, see Materials and Methods) is much shorter than the dimensions of the channel protein (Li et al., 1994, give the dimensions 80 × 80 $Å^2$ for the channel, thus 40 × 40 $Å^2$ for a K channel subunit), these charges are predicted to be located on the channel, relatively close to the voltage sensor.

In previous studies we have determined the functional surface charge density in seven K channels by analyzing Mg^{2+}- and Sr^{2+}-induced shifts of open probability curves. From a comparison between the net charge of the extracellular loops and the experimental values obtained for the charge densities of the different channels, we concluded that the relatively short and semiconserved extracellular loop between the fifth transmembrane segment and the pore region (S5–P loop) comprises the functional surface charges affecting the gating (Elinder et al., 1996; Elinder and Århem, 1998; Elinder et al., 1998). This is well in line with reported mutation experiments concerning the extracellular loops of K channels. Thus, charges on the S1–S2 loop (Grupe et al., 1990; Tseng et al., 1997) and the N-terminal end of the S3–S4 loop (Mathur et al., 1997) seem to have small effects on the gating. A charge at the C-terminal end of the S3–S4 loop (close to the voltage sensor S4) is, not unexpectedly, more influential (Tseng et al., 1997). It should be noted, however, that, in the wild-type K channels investigated here, the C-terminal residues of this loop are uncharged (see Gutman and Chandy, 1995). The largest influence on the voltage sensor has been noted for the S5–P loop (Talukder et al., 1995). Finally, the P–S6 loop does not seem plausible as the main determinant of the functional charge density because of its small interchannel variability and relative absence of charged residues.

In the present study, we extend the S5–P loop hypothesis further by determining the role of the individual charges of the S5–P loop. This is done by correlating the experimentally estimated surface potentials in previous investigations and the primary structure data. The results suggest that the N-terminal end of the S5–P loop has an α-helical structure, beginning with an absolutely conserved glutamate, located at a distance of 5–6 Å from the voltage sensor of the channel. The method discussed here can be seen as a complement to toxin-binding/site-directed-mutagenesis approaches to map structural details of voltage-gated channels.

MATERIALS AND METHODS

The relation between charge density (σ) and surface potential ($\psi(0)$) is described by the Grahame (1947) equation,

$$\sigma^2 = 2\varepsilon_r\varepsilon_0 RT \sum_i c_i[\exp(-z_i F\psi(0)R^{-1}T^{-1}) - 1], \quad (1)$$

where ε_r is the dielectric constant of the medium (80 in water), ε_0 is the permittivity of free space (8.85×10^{-12} Fm^{-1}), c_i is the bulk concentration (see below) and z_i is the valence of the ith ionic species in the extracellular solution. R, T (= 293 K), and F have their usual thermodynamic significance. The extracellular Ringer solution consisted of (in mM): 115 NaCl, 2.5 KCl, and 2.0 $CaCl_2$. The buffer (5 mM TRIS adjusted to pH 7.2) was not included in the calculations. Although Eq. 1 is strictly valid only for a uniformly smeared charge, it has been shown that the equation can be used as an approximation for charge densities more negative than −0.16 elementary charges per nm^2 (e nm^{-2}; Peitzsch et al., 1995). In the present investigation, the charge density analyzed was found to be more negative than this value for all channels but Kv3.4.

Received for publication 28 October 1998 and in final form 11 June 1999.

Address reprint requests to Peter Århem, The Nobel Institute for Neurophysiology, Department of Neuroscience, Karolinska Institutet, S-171 77 Stockholm, Sweden. Tel.: +46-8-728-6903; Fax: +46-8-34-9544; E-mail: peter.arhem@neuro.ki.se.

© 1999 by the Biophysical Society

0006-3495/99/09/1358/05 $2.00

The Debye length ($1/\kappa$) is described by

$$1/\kappa = \left(\frac{\varepsilon_r \varepsilon_0 RT}{(F^2 \sum_i c_i z_i^2)} \right)^{0.5}, \quad (2)$$

and is 9 Å in the present Ringer solution.

The nonanalytical solution of Eq. 4 (see below) constrained by the condition $\Psi_m \geq 0$ was found by a least-square procedure. Arbitrarily positive values for Ψ_m were used as initial values and the root mean square (rms) difference between calculated $\psi(0)$ values and experimental values was determined. The Ψ_m values were then changed one by one in small steps (each down to 0.1% of its value) until a change did not improve the fit. Normally, the iterative procedure halted after 10–20 rounds of all Ψ_m values. Tests of this procedure by introducing new initial values showed that the set of Ψ_m values obtained were unique.

RESULTS

The following analysis is based on the assumption that the functional surface potentials $\psi(0)_n$, calculated from the metal ion-induced shifts for the *n* different channels, represent the surface potentials at the voltage sensor. This does not seem unreasonable because the Grahame equation (Eq. 1) has been shown to be valid under the present conditions (see Materials and Methods), and because contributions from voltage sensor charges to $\psi(0)$ are expected to be of similar size (shifts for all channels measured at an open probability of 0.25, thus, when the channels are in open or close-to-open states). Assuming further that the analyzed S5–P loop has a similar secondary structure and location with reference to the voltage sensor in all investigated channels, we obtain the equation,

$$\psi(0)_n = \sum_m \Psi_m z_{mn}, \quad (3)$$

where Ψ_m is the potential contribution for an elementary charge *e* at the *m*th residue of the S5–P loop, and z_{mn} is the valence of the *m*th residue of the *n*th channel. Because a previous study (Elinder et al., 1998) suggested that the functional surface charges mainly are located at the N-terminal end of the S5–P loop, in the present analysis, we restricted the calculations to the eight first residues (shown in Table 1).

Applying Eq. 3 to the sequences in Table 1, assigning a charge of −1 to glutamate and aspartate, a charge of +1 to lysine and arginine, and a charge of +0.5 to histidine, we obtain the system of equations,

$$\begin{aligned}
\psi(0)_1 &= -\Psi_1 - \Psi_5 = -44\\
\psi(0)_2 &= -\Psi_1 - \Psi_3 - \Psi_4 - \Psi_6 + \tfrac{1}{2}\Psi_8 = -55\\
\psi(0)_3 &= -\Psi_1 - \Psi_3 - \Psi_4 - \Psi_5 - \Psi_6 + \tfrac{1}{2}\Psi_8 = -62\\
\psi(0)_4 &= -\Psi_1 - \Psi_3 + \tfrac{1}{2}\Psi_5 + \tfrac{1}{2}\Psi_8 = -30\\
\psi(0)_5 &= -\Psi_1 - \Psi_3 - \Psi_4 - \Psi_6 = -45\\
\psi(0)_6 &= -\Psi_1 + \Psi_2 - \Psi_3 - \Psi_4 - \Psi_5 - \Psi_6 + \Psi_8 = -30\\
\psi(0)_7 &= -\Psi_1 + \Psi_2 + \Psi_6 = -20.
\end{aligned} \quad (4)$$

This system has a unique solution ($\Psi_1 = 37$, $\Psi_2 = 42$, $\Psi_3 = -13.5$, $\Psi_4 = -3.5$, $\Psi_5 = 7$, $\Psi_6 = 25$, and $\Psi_8 = -20$ mV). A problem with this solution is that it includes negative values, implying that a negative charge can act as a positive charge on the voltage sensor. This is difficult to understand in terms of a mechanistic-electrostatic model. However, because an analytic solution to the equations above is very sensitive to deviations in $\psi(0)$, i.e., to measurement errors, we introduce the condition $\Psi_m \geq 0$ and solve the system numerically by a least square procedure, minimizing the rms difference between experimental and predicted $\psi(0)$ values (see Materials and Methods; for an evaluation of the sensitivity of the constrained case, see Appendix). The resulting values are $\Psi_1 = 38$, $\Psi_2 = 22$, $\Psi_3 = 0$, $\Psi_4 = 13$, $\Psi_5 = 8$, $\Psi_6 = 0$, and $\Psi_8 = 3$ mV and are plotted in Fig. 1 (rms difference = 4.3 mV). As seen from Fig. 1, the relation between the voltage contribution at the sensor and the site is described by a damped oscillation. The surface charge densities predicted from the values above show good agreement with those experimentally obtained as demonstrated in Fig. 2.

We thus suggest that the N-terminal residues, most conspicuously the absolutely conserved first residue glutamate, are the main functional surface charges of the K channel. The shape of the voltage contribution versus site curve suggests that every third residue of the S5–P loop is inac-

TABLE 1 S5–P sequences and experimental data of channels analyzed in the present investigation

Type of Channel	Residue Number 1	2	3	4	5	6	7	8	Experimental: Charge Density (e nm^{-2})	Experimental: Surface Potential (mV)	References
Shaker	**E**	A	G	S	**E**	N	S	F	−0.27	−44	Elinder et al., 1998
rKv1.1	**E**	A	**E**	**E**	A	**E**	S	*H*	−0.37	−55	Elinder et al., 1996
xKv1.1	**E**	A	**E**	**E**	**D**	**E**	S	*H*	−0.45	−62	Elinder and Århem 1998
rKv1.5	**E**	A	**D**	N	*H*	G	S	*H*	−0.17	−30	Elinder et al., 1996
rKv1.6	**E**	A	**D**	**D**	V	**D**	S	L	−0.28	−45	Elinder et al., 1996
rKv2.1	**E**	*K*	**D**	**E**	**D**	**D**	T	*K*	−0.17	−30	Elinder et al., 1996
rKv3.4	**E**	*R*	I	G	A	*R*	P	S	−0.11	−20	Elinder et al., 1996

The first eight residues of the N-terminal end of the S5-P loop and experimental estimations of surface charge density and corresponding surface potential for the seven K channels discussed in the present investigation. Amino acid residues denoted by single-letter code. Negatively charged residues in bold, positively charged in italics (for assigned values see text). Sequence sources listed in Elinder et al. (1998).

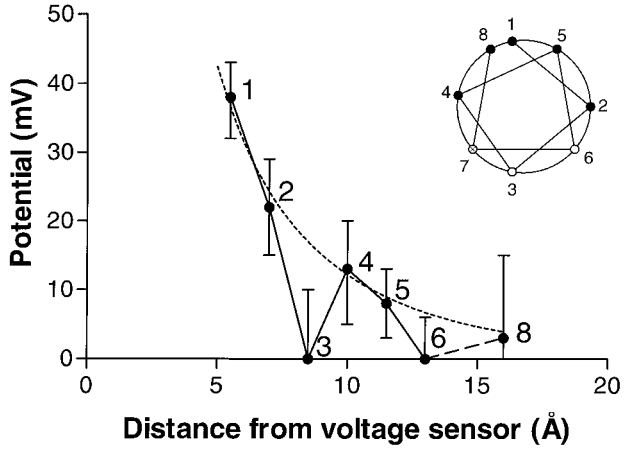

FIGURE 1 Site-dependent surface potential contribution of charges in the N-terminal end of the S5–P loop. Figures denote residue numbers as in Table 1. Values calculated from data in Table 1 by a least square procedure described in the text. The dashed line is the best fit of potential values for residue numbers 1, 2, 4, 5, and 8 to Eq. 2, expressed in distance from the voltage sensor. Interresidue distance is assumed to be 1.5 Å. The inset shows an α-helical wheel with upper residues (*filled symbols*), assumed to be exposed to the extracellular solution, and the lower residues (*open symbols*), assumed to be nonexposed. The status of residue 7 is undetermined (see text).

cessible to metal ion screening in the extracellular solution. An obvious explanation for such an effect pattern is an α-helical structure of the N-terminal end of the S5–P loop, although, of course, other conformations are possible. The implications of this suggestion are explored below.

DISCUSSION

By correlating primary structure data with surface potentials calculated from experimental data for seven voltage-gated K channels, we have estimated the electrostatic contribution of single residues in the S5–P loop to the surface potential at the voltage sensor S4. In the following, we will use these values to 1) discuss the exposure of these residues to the external solution in relation to results from other studies, 2) estimate the distance between the exposed residues and the voltage sensor, and finally, 3) discuss a structural hypothesis and its relation to a recent x-ray crystallographic structure of a bacterial K channel. In the Appendix, we will discuss the reliability of our calculations made in the Results section.

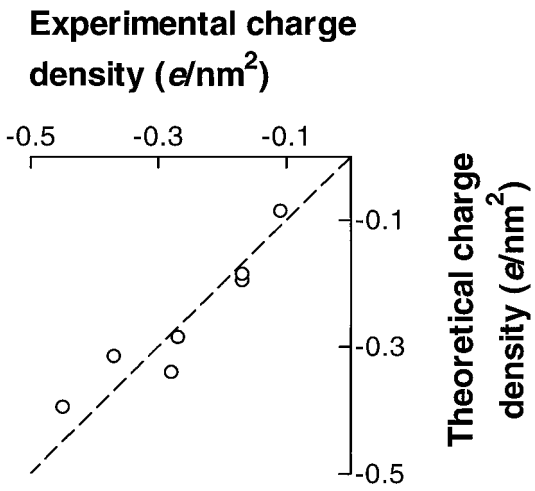

FIGURE 2 Experimentally estimated charge densities (see Table 1) versus theoretical charge densities (predicted from the calculated potential contribution values) for the seven channels in Table 1. The surface potential was derived from the potential contribution values and the charge density from the surface potential by Eqs. 1 and 3. The dashed line denotes a 1:1 relation.

The exposure pattern

The present results thus suggest that residues numbers 1, 2, 4, 5 and 8 are exposed to the external solution, while residues 3 and 6 are not. This is well in line with results from reported binding studies. Analyses of effects of charybdotoxin, Zn^{2+} and agitoxin2 on mutated channels show that residues 1, 2, 4, 5 and 8 of the S5–P loop are exposed to the toxin, while residues 3, 6, and 7 are not (MacKinnon et al., 1990; Talukder et al., 1995; Gross and MacKinnon, 1996; Krovetz et al., 1997). It should be noted that results for residues 2 and 6 contradicting the results mentioned above have also been reported (Gross and MacKinnon, 1996). However, as we will discuss below, these residues may be located at the border between exposed and nonexposed regions and therefore conflicting results are not unexpected.

Residue distances to the voltage sensor

Using the calculated potential contribution values, it is possible to roughly estimate the distance between the S5–P loop sites and the voltage sensor. We made use of the equation below, describing the potential $\psi(r)$ at the distance r from an elementary charge e, assuming that the charge is located at the border between a low-dielectric (membrane) and a high-dielectric (water) medium (McLaughlin, 1989)

$$\psi(r) = 2e \exp(-\kappa r)/(4\pi\varepsilon_0\varepsilon_a r). \quad (5)$$

ε_0 is the permittivity of free space (8.85×10^{-12} Fm^{-1}), ε_a is the relative dielectric constant of the aqueous phase (80), and κ is the inverse of the Debye length in the aqueous phase (9 Å in Ringer solution, see Materials and Methods). (The solution to this equation is shown in Fig. 1). Fitting the estimated nonzero Ψ_m values (exposed residues) to the curve, the following distances (in Å) are obtained: 5.3 (residue number 1), 7.4 (2), 9.7 (4), 12.1 (5), and 17.5 (8). Clearly, the underlying assumptions for this calculation are simplistic. Assuming a more complex structure around the sensor, involving crevices in the channel protein, the estimation will change (the lower limit being set by the case of free charges in solution, which reduces the values above by 50%). However, until more structural details of the S4

region are available, the present calculation may serve as guideline for future experimental tests.

A structural hypothesis

As mentioned above, an obvious explanation to the present results is the hypothesis of a helical structure of the N-terminal end of the S5–P loop. Assuming that the longitudinal axis of the helix is perpendicular to the voltage sensor (giving an interresidue distance of 1.5 Å), the site-specific potential contributions Ψ_m well fit Eq. 5 when the distance between residue 1 and the voltage sensor is 5.5 Å (Fig. 1). The associated helical wheel in Fig. 1 shows that residues 2 and 6 are located at the border between exposed and nonexposed regions, possibly explaining the conflicting results discussed above. Figure 3 shows that only minor modifications are required to include a helical S5–P loop (*right panel*) in the structural model of the *Shaker* channel proposed by Durell et al. (1998) (*left panel*). Note that the first two residues (1 and 2), shown to influence the voltage sensor most in the present investigation, are located relatively close to S4.

The helix suggestion seems to be contradicted by results from the recently presented crystal structure of a bacterial K channel (KcsA from *Streptomyces lividans*) in which the N-terminal part of S5–P (called turret by Doyle et al., 1998) is a random coil rather than an α-helix (Doyle et al., 1998). However, it should be pointed out that the KcsA channel contains a proline (at the top of the turret; position 5) and prolines are known to break α-helical structures. This proline residue is absent in all the K channels included in the present analysis. Thus, it cannot be excluded that the S5–P loop in these channels has a helical structure. In contrast to the KcsA channel, the presently analyzed channels are voltage regulated and a helical structure of S5–P may be of relevance for the voltage-sensing S4 machinery, for instance, by stabilizing the S5–P loop in a position not to disturb the S4 movement. α-helices have significant dipole moments (see Nakamura, 1996) and are thus stabilized by a negative charge in the N-terminal end and a positive charge in the C-terminal end. It is noteworthy that the negative glutamate residue at position 1 is conserved in all known Kv channels (Gutman and Chandy, 1995), and that, in four out of the seven channels investigated in the present report, the residue at position 8 carries a positive charge.

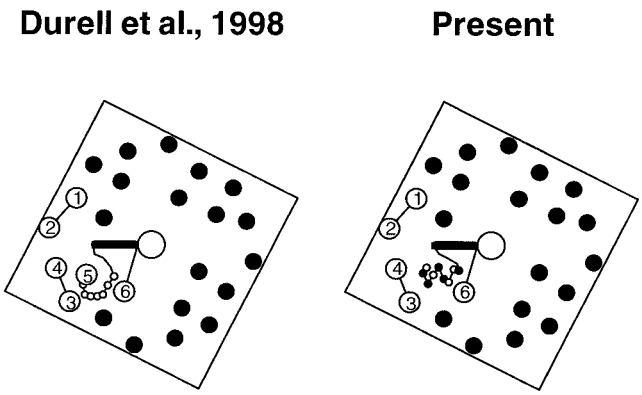

FIGURE 3 Schematic diagram of the extracellular surface of a Kv channel. One (of four) subunit is shown in more detail. Small circles on the loop between S5 and S6 are the individual amino acid residues investigated in the present study. The thick bar indicates the pore helix (see Doyle et al., 1998). The ion-permeating pore is located in the middle of the channel. Loops connecting S1 with S2 and S3 with S4 are added for clarity. The length of one side of the channel is about 7 nm. The left panel shows the principal features of the molecular model of Durell et al. (1998). Note that residue 1 is within S5. The right panel shows the modified model based on the present results. Filled symbols denote exposed, and unfilled symbols denote nonexposed, residues. Note that the residue before the glutamate in position 1 is also included to show where S5 ends.

Concluding remark

In summary, we have presented results from a correlation analysis yielding data on site-specific effects on the gating of K channels, unexpectedly suggesting an α-helical structure of the S5–P loop. The results can also be used to predict the functional surface potential (and consequently the surface charge density) of other channels, not yet experimentally analyzed. Using reported sequence data (Gutman and Chandy, 1995), most Kv1 channels (including *Shaker*) are predicted to have a density of about $-0.3e$ nm^{-2}; Kv2 (including Shab) and Kv1.5 channels, a density of about $-0.2e$ nm^{-2}; Kv3 (including Shaw), Kv4 (including Shal), and Kv1.7 channels, a density of about $-0.1e$ nm^{-2}.

Previous electrostatic mapping investigations have focused on the pore region rather than on the voltage sensor region and involved reciprocal mutations on the K channel and the specific blocker charybdotoxin (Stocker and Miller, 1994). The present correlation analysis provides a novel method to map structural details of voltage-gated channels, complementing the toxin-binding/site-directed-mutagenesis approach but avoiding possible complications caused by mutation-induced structural changes. It should be directly applicable to the mapping of internal surface charges influencing gating and the charges affecting conductance.

APPENDIX: RELIABILITY OF THE SOLUTION

The results above critically depend on the validity of the approach used. How sensitive is the solution obtained (the damped oscillation in Fig. 1) to experimental uncertainties? We approached this problem in two ways.

First, we investigated how sensitive the Ψ_m-values were to an increased deviation from the experimental values. We calculated values for ψ_m when the rms value from the calculations above (4.3 mV) was allowed to increase by 20% (to 5.2 mV). The bars in Fig. 1 indicate the limiting values obtained. Although it is possible to construct a curve within the bars that is not a damped oscillation, all individual solutions were damped oscillations of the same magnitude as that shown in Fig. 1 (data not shown).

Second, we investigated how sensitive the Ψ_m-values were to changed experimental values. We calculated values for Ψ_m when the experimental surface potentials were allowed to deviate by 10%. Thus, each experimental value was assumed to be either 10% higher or 10% lower than that given in Table 1. By solving the resulting equation system for all of the 128 ($= 2^7$) combinations, we could show that the site-dependent potential contribution still is described by a damped oscillation of the same magni-

tude as that in Fig. 1 (data not shown). In conclusion, the solution obtained seems relatively insensitive to experimental uncertainties.

Another, but related, question is how unique the set of amino acid sequences of Table 1 is in giving a solution that shows the found fit to the experimental values? Can other sequences, located on other extracellular loops, give solutions of equally good or even better fits? To investigate this, we compared the rms value obtained above (4.3 mV) with corresponding calculations for arbitrary amino acid sequences constructed with the help of the random generator of the computer. The arbitrary sequences were constructed on the assumption that all amino acid residues were equally frequent. Thus, 10% were assigned a charge of −1, 10% a charge of +1, and 5% a charge of +0.5. The result of the calculations showed that the probability to find another set of residue sequences that gives a solution that better fits the experimental values than that of Table 1 is very small. Out of 10,000 sets of arbitrary sequences, only 20 yielded rms values smaller than 4.3 mV, that is, the probability of finding a set of sequences giving a solution of a better fit to the experimental data than that of Table 1 is 0.2%. Furthermore, the 1% best cases included rms values of up to 11 mV, far above 4.3 mV. Even more convincing is the case when making corresponding estimations for five-residue sequences. Such an estimation seems justified by the fact that charges at positions 6, 7, and 8 only marginally contribute to the surface potential at the sensor, well in line with the negligible increase of rms value when comparing the five-sequence-residue case with the eight-residue case (4.4 mV versus 4.3 mV). The calculations showed that, out of 100,000 sets of arbitrary sequences, only three yielded smaller rms values than 4.4 mV, that is, the probability to find a set of sequences better fitted to the experimental values was 0.003%. The 1% best cases included rms values of up to 20 mV. In conclusion, these estimations suggest that the specific amino acid sequences of the investigated S5–P loops are unique in giving a solution that fits the experimental values.

This work was supported by grants from the Swedish Medical Research Council, The Swedish Society of Medicine, Åke Wibergs stiftelse and Hjärnfonden. Constructive criticism from Dr. Peter Larsson is gratefully acknowledged.

REFERENCES

Baker, P. F., and K. A. Rubinson. 1975. Chemical modification of crab nerves can make them insensitive to the local anaesthetics tetrodotoxin and saxitoxin. *Nature*. 257:412–414.

Doyle, D. A., J. M. Cabral, R. A. Pfuetzner, A. Kuo, J. M. Gulbis, S. L. Cohen, B. T. Chait, and R. MacKinnon. 1998. The structure of the potassium channel: molecular basis of K^+ conduction and selectivity. *Science*. 280:69–77.

Durell, S. R., Y. Hao, and H. R. Guy. 1998. Structural models of the transmembrane region of voltage-gated and other K^+ channels in open, closed, and inactivated conformations. *J. Struct. Biol*. 121:263–284.

Elinder, F., and P. Århem. 1998. The functional surface charge density of a fast K channel in the myelinated axon of *Xenopus laevis*. *J. Membrane Biol*. 165:175–181.

Elinder, F., M. Madeja, and P. Århem. 1996. Surface charges of K channels. Effects of strontium on five cloned channels expressed in *Xenopus* oocytes. *J. Gen. Physiol*. 108:325–332

Elinder, F., Y. Liu, and P. Århem. 1998. Divalent ion effects on the *Shaker* K channel suggest a pentapeptide sequence as determinant of functional surface charge density. *J. Membrane Biol*. 165:183–189.

Frankenhaeuser, B. 1960. Sodium permeability in toad nerve and squid nerve. *J. Physiol. (Lond.)*. 152:159–166.

Frankenhaeuser, B., and A. L. Hodgkin. 1957. The action of calcium on the electrical properties of squid axons. *J. Physiol. (Lond.)*. 137:218–244.

Grahame, D. C. 1947. The electrical double layer and the theory of electrocapillarity. *Chem. Rev.* 41:441–501.

Gross, A., and R. MacKinnon. 1996. Agitoxin footprinting the *Shaker* potassium channel pore. *Neuron*. 16:399–406.

Grupe, A., K. H. Schröter, J. P. Ruppersberg, M. Stocker, T. Drewes, S. Beckh, and O. Pongs. 1990. Cloning and expression of a human voltage-gated potassium channel. A novel member of the RCK potassium channel family. *EMBO J*. 9:1749–1756.

Gutman, G. A., and K. G. Chandy. 1995. Voltage-gated K^+ channels. *In* Handbook of Receptors and Channels. Ligand- and Voltage-Gated Ion Channels. R. A. North, editor. CRC Press, Boca Raton, FL. 1–71.

Krovetz, H. S., H. M. A. VanDongen, and A. M. J. VanDongen. 1997. Atomic distance estimates from disulphides and high-affinity metal-binding sites in a K^+ channel pore. *Biophys. J*. 72:117–126.

Li, M., N. Unwin, K. A. Stauffer, Y. N. Jan, and L. Y. Jan. 1994. Images of purified *Shaker* potassium channels. *Curr. Biol*. 4:110–115.

MacKinnon, R., and C. Miller. 1989. Mutant potassium channels with altered binding of charybdotoxin, a pore-blocking peptide inhibitor. *Science*. 245:1382–1385.

MacKinnon, R., L. Heginbotham, and T. Abramson. 1990. Mapping the receptor site for charybdotoxin, a pore-blocking potassium channel inhibitor. *Neuron*. 5:767–771.

Mathur, R., J. Zheng, Y. Yan, and F. J. Sigworth. 1997. Role of the S3–S4 linker in *Shaker* potassium channel activation. *J. Gen. Physiol.* 109: 191–199.

McLaughlin, S. 1989. The electrostatic properties of membranes. *Ann. Rev. Biophys. Chem*. 18:113–136.

Nakamura, H. 1996. Roles of electrostatic interaction in proteins. *Quart. Rev. Biophys*. 29:1–90.

Peitzsch, R. M., M. Eisenberg, K. A. Sharp, and S. McLaughlin. 1995. Calculation of the electrostatic potential adjacent to model phospholipid bilayers. *Biophys. J*. 68:729–738.

Sigworth, F. J., and B. C. Spalding. 1980. Chemical modification reduces the conductance of sodium channels in nerve. *Nature*. 283:293–295.

Stocker, M., and C. Miller. 1994. Electrostatic distance geometry in a K^+ channel vestibule. *Proc. Natl. Acad. Sci. USA*. 91:9509–9513.

Talukder, G., M. M. Tamkun, and N. L. Harrison. 1995. A role for the "pre-pore" region of voltage-dependent K^+ channels in gating and zinc modulation. *Soc. Neurosci. Abstr*. 21:1033.

Tseng, G.-N., J. Xia, and M. Jiang. 1997. Role of charges on extracellular loops in the voltage-dependence of gating of Kv1.4. *Biophys. J*. 72:A29.